Hybrid Modeling and Design Optimization of Chip Level of µs Long Optical Delays for Realization of Integrated Optoelectronic Circuits

Kai Wei and Afshin S. Daryoush[*]

Abstract—Integrated time delays are important for self-forced oscillation techniques in opto-electronic oscillators (OEO). Add-drop filters (ADFs) resonators using optical waveguide coupled to micro-ring resonators (MRR) are suitable for integrated optical time delays but suffer from a limited expected delay. 2-dimensional (2-D) photonic crystals (PhCs) with line defect are employed as confined optical waveguide to realize ADF resonators where longer optical delays than standard homogenous resonators are achieved by leveraging the slow-light effect. Moreover, achieving time delay up to microseconds (µs) is envisioned by cascading multiple identical ADFs based on dispersive 2-D PhC micro-resonators. The focus of this paper is to devise a hybrid modeling procedure for accurate calculations of achieved time delays in various complex structures, while a combined electromagnetic modeling and analytical calculation technique overcomes a substantial computational resources and long computation times for a brute forced full-wave design and modeling. This innovative hybrid modeling for time delay estimation of cascaded ADFs is proposed for the first time to optimize physical design within short time period. First, transfer function performance of a homogenous ADF resonator is simulated using finite-difference-time-domain (FDTD) for both the full structure and structures with bi-fold symmetry and compared against proven analytical solutions to demonstrate the accuracy of bi-fold symmetry while the computational resources are economized. The same modeling procedure is then extended to predicting performance of 2-D PhC based ADF resonator by quantifying key physical parameters of coupling factor, complex optical propagation constant, and optical transfer function for ADF resonator for the ring radius of curvature about 1.5 µm with various coupling gaps between feed waveguide and resonator guide. These parameters and the effective group index calculated by OptiFDTD software are applied to the analytical expressions to estimate single 2-D PhC ADF and attain a simulated time delay of 200 ps. The estimated time delay of 70 cascaded 2-D PhC based ADF resonators with R of 100 µm is estimated to be about 925 ns for the on-resonance frequency of 1534 nm.

1. INTRODUCTION

Integrated optoelectronic circuit (IOEC) implemented using Si-photonic integration circuits (PIC) is of great interest for large scale monolithic circuits as analog beamforming network [1] in modern telecommunication and remote sensing system. A system-on-chip (SoC) is desired due to its compact size, low cost, low harsh environmental sensitivity, and improved performance in terms of optical interconnect losses compared to hybrid integrated circuit designs. In the current foundry service, most passive optical components are developed on Si-photonic (SiP) using either Si_3N_4 or SiO_2 platforms for low optical loss and capability with highly intense nano-scale integration [2], while all active sources (i.e., semiconductor optical amplifiers and lasers) or efficient photodetectors (PD) are based on III-V (e.g., InGaAsP/InP) material [3]. A full integrated SoC is realized by heterogeneous integration procedures [4].

An immediate practical application of IOEC is in the area of integrated optoelectronic oscillator (IOEO), where highly stable and low phase noise RF oscillators are widely used in coherent detection systems [5] or as an optical clock signal for high-speed analog/digital conversion (ADC) [6, 7]. Unfortunately, the preliminary IOEO using directly modulated laser (DML) and an 8.97 mm long optical delay line (ODL) with its chip size of $5 \times 6\,\mathrm{cm}^2$ suffers from poor phase noise (e.g., $\sim -60\,\mathrm{dBc/Hz}$ at 10 kHz offset of 8.87 GHz) thus far [8] due to its associated extremely low Q-factor of the IOEO as result of a very limited optical time delay ($\sim 95\,\mathrm{ps}$). Moreover, even though an alternative IOEO RF source has been recently demonstrated as a compact size design approach using multi-mode laser techniques [9] with extremely low phase noise (viz., $\sim -110\,\mathrm{dBc/Hz}$ at 10 kHz offset of 26.7 GHz) using self-mode locking (SML) techniques [10, 11], the calculated close-in to carrier phase noise performance under adverse condition of having random phase error of within $\pm 0.5°$ per mode causes additional phase noise degradation [12]. Therefore, the concept of self-forced oscillation of SILPLL [7, 13] is modularly combined with SML to experimentally demonstrate timing jitters of under 2 fs [14] that could meet as many as 8 effective number of bits (ENOB) at 40 GS/s for a high-efficient ADC application [15]. However, the improved performance using self-forced techniques requires a minimum optical delay element of 1 µs scale time delays, and such component IOEO chip realization using SML combined with SEILDPLL [7] has to be analyzed prior to full chip level demonstration of IOEO.

On-chip implementation of the required µs optical delays is challenging, and the spiral-like compact ODL [8] for optimized performance in principle is not an ideal solution since it demands a large chip footprint. Linear chirped fiber Bragg grating (LCFBG) is a simple structure that achieves relatively large time delay (i.e., 200 ps [16] using modular components); however, the achieved delay is still limited by the RF modulation bandwidth of the optical carrier. Alternative approaches, like Whispering Gallery Mode (WGM) resonators [17] or Fabry-Perot resonators [18], are also attractive miniaturization solutions to high-Q storage elements, which with a Q-factor of over 10^8 under critical light coupling could reach an RF loaded Q-factor of under 10^4 [19]. To achieve highly compact integration, a high-Q microdisk resonator (MDR) based Si-IOEO in [8] is designed by heterogeneous integration of InP on SiP that is combined with $SiGe$ HBT technologies. This seamless integration of electronic and optical circuits on a single chip is estimated with a chip size of about $1.3 \times 2\,\mathrm{mm}^2$. In addition, micro-ring resonators (MRRs) of all-pass or add-drop (cf. Figure 1(a)) configurations could achieve moderate optical delays, and a practical design realization of MRR based add-drop filter (ADF) is depicted in Figure 1(b) [20]; however, MRRs are subject to the radius of the ring waveguide that determines the free-spectral range (FSR), finesse of the resonator (F), and transmission characteristics (H) of ADF. In practice, optical bending loss and 3-dB bandwidth of a ring that is specially associated with the ADF structure should be optimized to accommodate the efficient coupling of the modulated optical modes to the drop port [21].

(a)   (b)   (c)
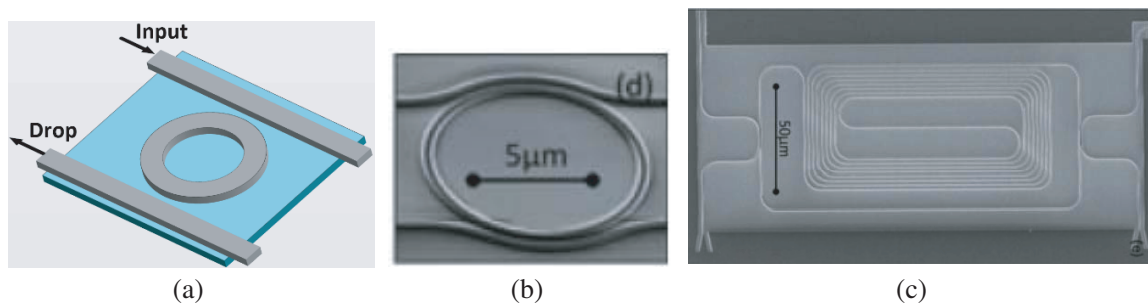
Figure 1. (a) Configuration of homogenous ADF resonators and physical images of single ADF with (b) short delay [20] and (c) long delay using serpentine design [20].

Optimum integrated chip design based on hybrid electromagnetic field modeling of cascaded ADF using MRR is the purpose of this paper. Particularly, in this paper a hybrid modeling method of 2-D PhC based ADF that combines FDTD simulations and analytical solutions is presented to estimate the performance of the proposed 1 µs optical delay element without relying on computational resource challenges of full-wave modeling of the large diameter cascaded ADF structures. The system level

concept of transfer function H is introduced and considered for cascaded MRR based ADF. These designs and modeling are to be applied for the fully integrated self-electrical injection locked (SEIL) oscillation [7] combined with dual self-phase locked loop (DSPLL) oscillation [22] as demonstrated using integrated optical delays of up to about 1 μs. This paper presents the novelty of this computationally efficient optical delay design approach applied to a fully IOEO as proposed for realization of a self-forced multi-mode laser that employs the concept of SML and SEIL-DSPLL [14] for ultra-stable clocks.

2. BASELINE MODELING: HOMOGENOUS RING RESONATOR

2.1. Hybrid Modeling

An ADF resonator with a long-time delay using high Q MRR — depicted in Figure 1(a) — is employed for its low optical loss within periodic band-pass regions. When the ring waveguide is coupled to the two bus waveguides at ports 1 and 2, the input light is partly transmitted to the drop port (i.e., port 2) within an optical passband bandwidth. Hybrid modeling is to take advantage of the optical transfer function, H_{drop} for the drop port of ADF resonators to reduce the modeling time-period, while maintaining the accuracy in modeling of ADFs; H_{drop} is mathematically expressed by [23]

$$H_{drop} = \frac{-\sqrt{(1-\gamma_1)\,\kappa_1\,(1-\gamma_2)\,\kappa_2}\,e^{-(\alpha L/4 + j\pi n_g L/\lambda)}}{1 - \sqrt{(1-\gamma_1)\,(1-\kappa_1)\,(1-\gamma_2)\,(1-\kappa_2)}\,e^{-(\alpha L/2 + j2\pi n_g L/\lambda)}} \tag{1}$$

where $\kappa_{1\&2}$ are the coupling coefficients for each coupler, and $\gamma_{1\&2}$ are the coupling insertion loss in upper and lower coupling regions from bus to MRR. The excess optical loss value is estimated by calculating $1 - |S_{11}|^2 - |S_{12}|^2 - |S_{13}|^2 - |S_{14}|^2$ where the scattering parameter of 4-port optical MRR is S_{ij} — with $i\&j$ being integer numbers of 1, 2, 3, 4. Parameter α denotes the optical waveguide loss in Np/m which can be found by the FDTD simulation of unity length of lossy waveguide with complex refractive index of optical guide. L is the circumference of each ring waveguide, and n_g is the group refractive index of optical guide.

Among these parameters, the two parameters of group index (n_g) and coupling coefficient (κ) are the critical factors that determine the FSR, number of optical modes supported within MRR resonance, and associated wave propagation time delays. The effective refractive index (n_{eff}) of the fundamental mode inside the ridge waveguide structure versus wavelength (λ) of incident light is numerically calculated using OptiFDTD mode-solver [24]. Parameter n_g represents the waveguide dispersion with respect to λ, which is expressed by $n_{eff} - \lambda_0 \cdot \partial n_{eff}/\partial \lambda$. For a Si/SiO_2 ridged waveguide surrounded by Air with the ridge width and height of 400 nm and 180 nm, respectively, the group index of about 4.625 is calculated around $\lambda_0 = 1545$ nm.

On the other hand, the calculation of coupling coefficient is more complex as the coupling region is a curved function along the propagation direction. The analytical solution of *Marcatili* method presented in [25] is employed to estimate the coupling coefficient between the bus waveguide and ring waveguide. The coupling coefficient for TE-mode wave is modelled depending on the gap between MRR and optical waveguide, and the dependence is depicted in Figure 2.
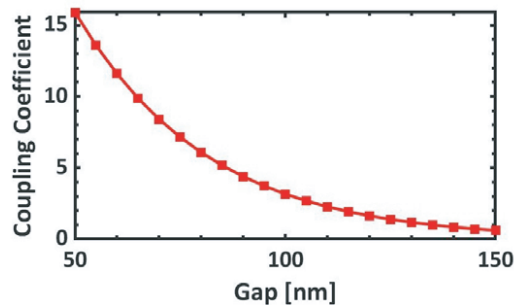
Figure 2. Coupling coefficient versus gap between bus/ring waveguide for $R = 1.7$ μm for wavelength of 1545 nm.

2.2. FDTD Modeling: Full-Structure vs Bi-Fold Symmetric Structure

A symmetric structure of single ADF can be reduced in physical size by taking advantage of perfect magnetic conductor (PMC as H wall) and perfect electric conductor (PEC as E wall) along the lines of symmetry of an MRR based ADF. The presented symmetric structure of Figure 1(a) is reduced to Figure 3, where PEC and PMC replace the bi-fold line of symmetry in the full structure. Computational resources required for high spatial resolution employed in accurate full-wave simulation of the structure shown in Figure 3 are significantly reduced even though one has to repeat a similar simulation four times with appropriate boundary constraints of PMC and PEC. Note that even/odd modes modeling technique is employed for these individual simulations; in particular, S_{11}^e and S_{11}^o are attained when the lines of symmetry across ports 1&2 and 3&4 are replaced by either PMC (cf. Figure 3(a)) or PEC (cf. Figure 3(b)) for even- and odd-mode excitations, respectively. Therefore, the scattering parameters of the coupler can be calculated by the reflection coefficient at the input port 1 obtained from the analysis of the structure as shown in Figure 3 and analytically expressed as [26]:

$$S_{21} = \frac{S_{14}^e - S_{14}^o}{2} = \frac{S_{11}^e - S_{11}^o}{2} \tag{2}$$

$$S_{41} = \frac{S_{14}^e + S_{14}^o}{2} = \frac{S_{11}^e + S_{11}^o}{2} \tag{3}$$

where S_{41} and S_{21} represent the optical insertion losses at through and drop ports, respectively.
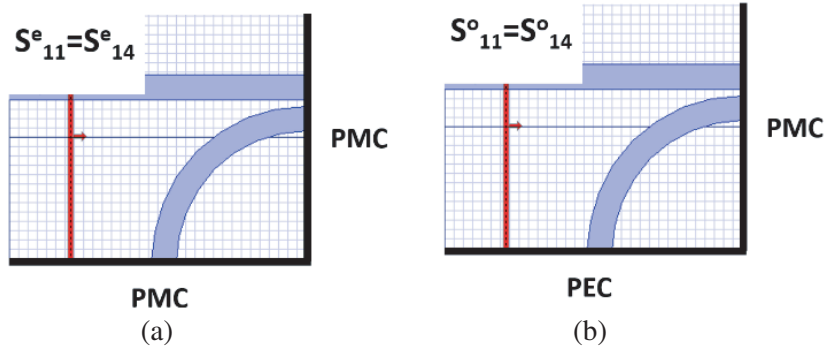
Figure 3. Analysis of an ADF using the bi-fold symmetry in OptiFDTD; (a) for even mode excitation, (b) for odd mode excitation.

To demonstrate the accuracy of this modeling approach, a Si/SiO_2 ADF resonator (i.e., modified from the default example of Getting_Started_Ring_Resonator.fdt in OptiFDTD 15 Samples folder [24]) is modeled, simulated, and compared against one another with radius $R = 1.7\,\mu\text{m}$ and gap of $55\,\text{nm}$ with simulated coupling insertion loss of 0.02 in Figure 4. The coupling simulation results of full-wave modeling of the complete structure are compared against multiple simulations of the quarter of the full structure using even and odd modes by employing PMC and PEC along the bi-fold symmetric planes. A 40-nm grid resolution is employed in FDTD simulation over wavelengths of 1520 nm to 1570 nm for the highest accuracy without significantly increased simulation time. The proposed hybrid modeling results are compared in terms of transmission in through and drop ports versus wavelength (cf. Figure 4). As depicted in Figure 4, a small error of 0.5% for the resonance wavelength is observed between the FDTD simulations of bi-fold symmetric structure of Figure 3 and the FDTD simulation of the full structure shown in Figure 1(a); this error is due to the boundary condition errors in FDTD simulation [25] for 40 nm spatial resolution. The hybrid modeling, on the other hand, perfectly matches the result of full-wave simulation; however, both bi-fold and full-structure FDTD simulations suffer more loss and lower Q-factor at the resonance wavelength than that obtained by the hybrid modeling due to a large mesh size of 40 nm that was used to speed up this simulation. More accurate results in FDTD simulation could be calculated using a higher grid resolution at cost of a longer simulation time (e.g., simulation time of about 20 hours using a 10-nm mesh size) that matches the H_{drop}. Therefore, the proposed hybrid modeling is a preferred solution to estimate on-resonance wavelength and insertion loss/phase performance in the ADF resonators.
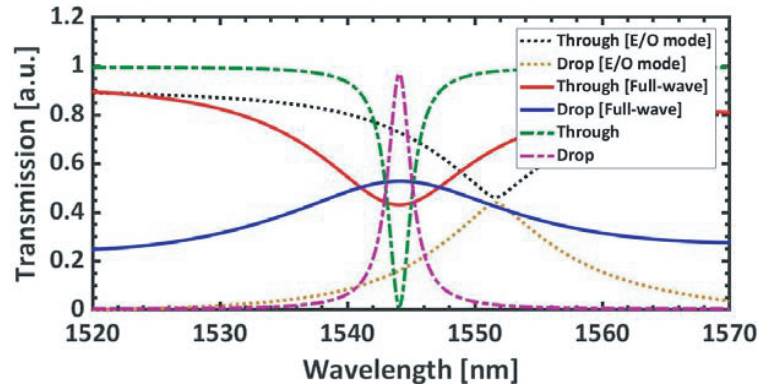
Figure 4. Transmission spectrum of ADF resonator using various simulation topologies.

The calculated optical time delay of the ADF resonator through drop port is estimated by taking derivative of the optical insertion phase from transfer function H presented in Eq. (1) with respect to angular frequency (i.e., $\partial\varphi_{drop}/\partial\omega$ where $\omega = 2\pi c/\lambda$). The simulated result of optical delay is depicted in Figure 5 versus wavelengths of 1520–1570 nm. The estimated optical insertion loss and time delay of a 3.4 μm in diameter ring are about 0.1 dB and 1 ps, respectively at the resonance wavelength of 1545 nm, which is not sufficient to replace the required optical delays in IOECs. Therefore, the first option is to use MRR of a larger diameter and employ a greater number as cascaded structure. A space saving format of serpentine MRR format is shown in Figure 1(c) that is still not sufficient for the IOEC. The other option of achieving longer time delays is to employ slow-light effect using 2-D PhC rather than employing the homogenous MRR. The first option was reported elsewhere [7], while the second approach is reported in the next section.
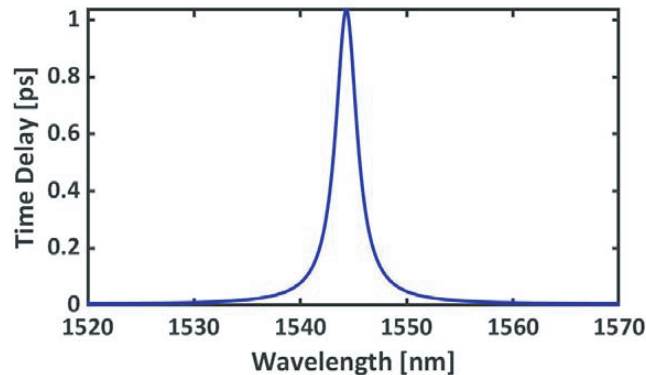
Figure 5. Calculated time delay through the drop port against wavelength using hybrid modeling for $R = 1.7$ μm, gap $= 55$ nm at wavelength of 1545 nm.

3. MODELING OF DISPERSIVE RING RESONATOR

3.1. Baseline Modeling of 2-D Photonic Crystal

Optical delays that exploit slow-light feature of 2-D photonic crystal (PhC) cavity resonators better meet the requirement of a compact integrated circuit of smaller dimensions than homogenous waveguides. The 2-D PhC ADF resonators are good candidates that combine the advantage of band-pass filtering of ADF resonators and slow-light structures of 2-D PhC dispersive medium. Figure 6(a) shows the 2-D rectangular lattice PhC slab design with an air substrate and a 20×19 Si-rod array in OptiFDTD

following design concepts reported in [27]. The PhC design parameters of a lattice constant of $a = 500$ nm with a filling factor $f = 0.177$ enable the on-resonance optical mode to propagate inside the slowlight region. The lattice constant and filling factor of this design are primarily modified values from [27] to shift the on-resonance wavelength to the dispersive region of the guided mode. The radius of 2-D PhC waveguide-based ring is $3 \times a$, and the overall dimension is about $10 \times 9\,\mu\mathrm{m}^2$. The number of rod rows between the defect bus waveguide and defect ring waveguide controls the coupling efficiency. Moreover, the initial defect ring waveguide is square-like, which is not the most efficient method of realizing low optical loss resonators. Therefore, scattering rods are added to the square ring resonator, which are located at lattice order locations of $(8, 8)$, $(8, 12)$, $(12, 8)$, $(12, 12)$ (cf. the inside rods highlighted by the red dot-line circles) to modify the square resonator into a hexagonal lattice $(a' = a/\sqrt{2},\ f' = \sqrt{2}f)$ for a quasi-circular pattern. Inside the photonic bandgap (PBG) region, there exists a guided band with normalized frequency ranging from 0.64 to 0.87 (cf. Figure 6(b)) calculated by PWE band solver in OptiFDTD. The effective group indices of the guided band are calculated (i.e., $c/(\partial\omega/\partial k)$) and plotted as a function of wavelength in Figure 6(c). Of particular interest is effective group index of 8.25 at 1534 nm, which is about 2 times larger than the homogenous design. Moreover, the designed radius is slightly smaller than that of the example shown in the previous section due to the selected lattice constant and filling factor of the 2-D PhC lattice which determine the projected guided mode inside the PBG region. Therefore, the operating optical wavelength in this case is slightly shifted, and the full-wave simulation is presented in Figure 7(a). Although the dispersive characteristics of all modes inside the slowlight region (viz. from ~ 1534 nm to ~ 1562 nm) are enhanced (cf. Figure 6(c)), the general ADF resonator structure adds passing band selectivity which is primarily controlled by the radius of resonator [23]. Therefore, the lattice constant and filling factor for the projected 2-D PhC

(a)

(b)   (c)
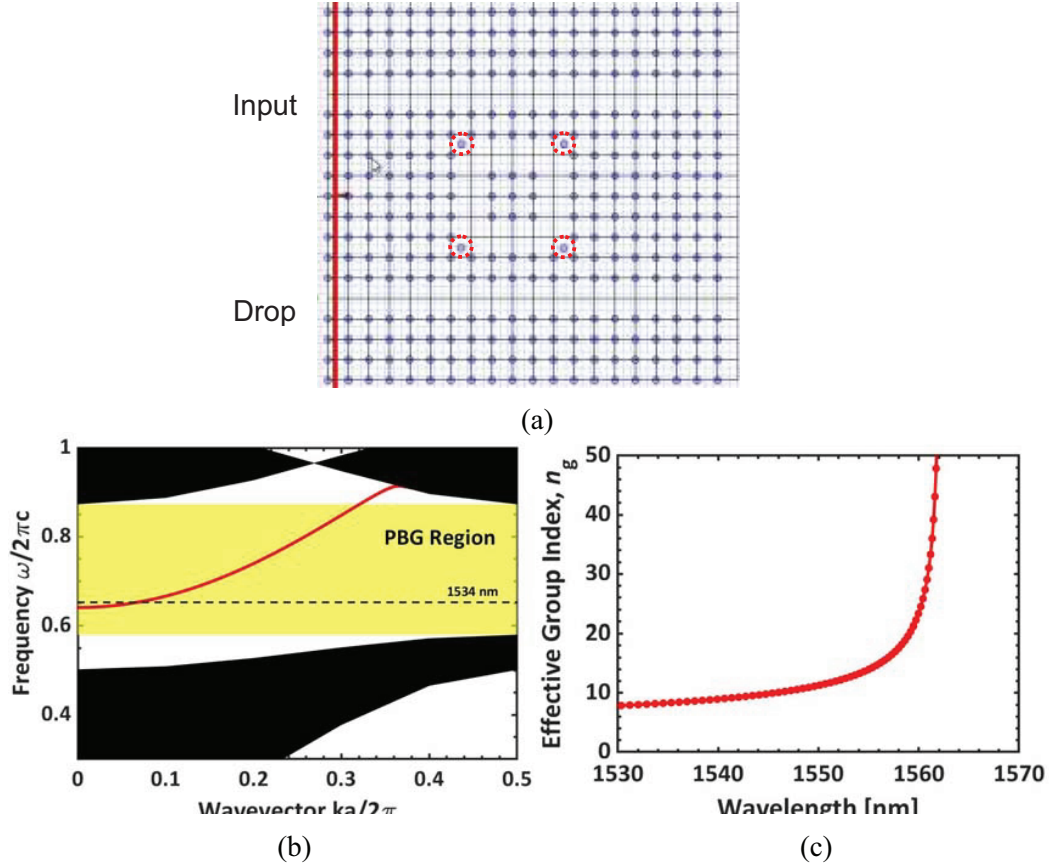
Figure 6. (a) Layout sketch of the 2-D PhC based ADF resonator after [27]. (b) Defect mode in ωk diagram. (c) Calculated effective group index.

(a)

(b)

(c)
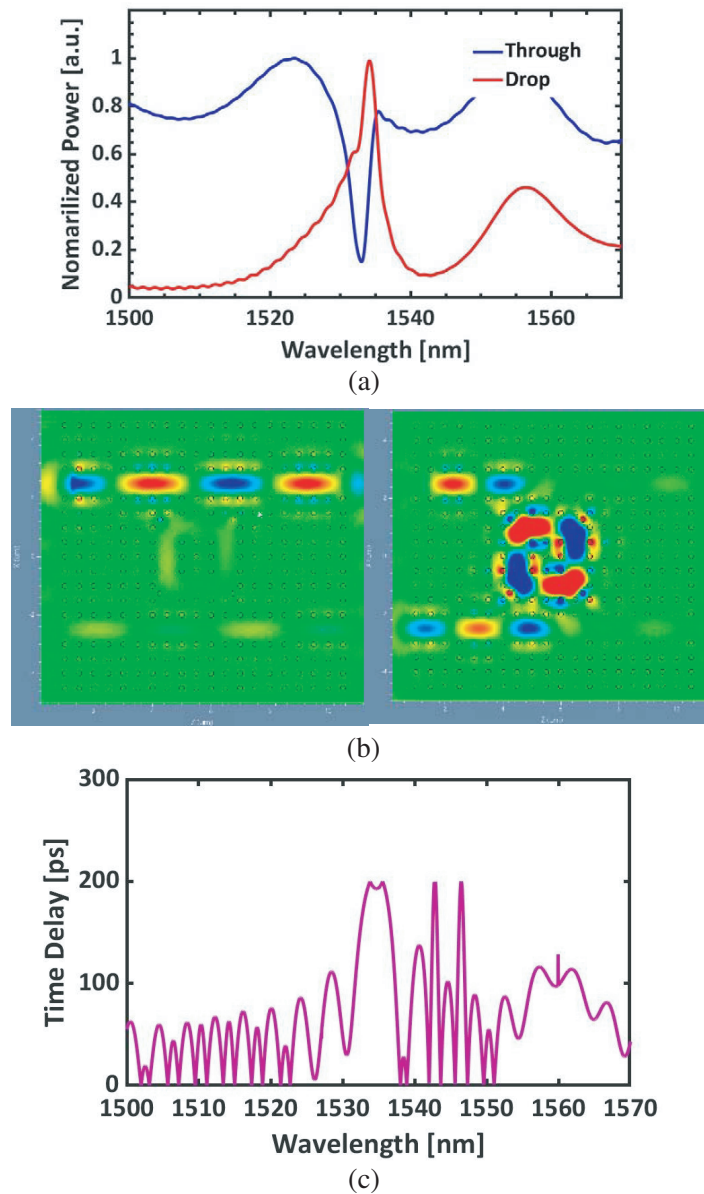
Figure 7. (a) Normalized transmission spectra of the designed 2-D PhC based ADF and (b) optical field for on resonance wavelength of 1534 nm (left) and off-resonance of 1523 nm (right), where red and blue show peak fields of in phase and out of phase and yellow corresponds to a 10 dB lower than peak optical field. (c) Calculated time delay for the drop port versus wavelength.

design and the radius of the defect-line ring waveguide should be redesigned for a practical case that enables the operating wavelength (e.g., 1550 nm) to experience both on-resonance and slowlight effects.

Figure 7(a) shows OptiFDTD simulation results of the normalized transmission spectra for drop and through ports of the designed lossless 2-D PhC ADF resonator; an optical insertion loss of about 0.04 dB is calculated at 1534 nm for drop port of a single ADF resonator implemented with 2-D PhC based dispersive medium due to an estimated coupling insertion loss of $\gamma = 6 \times 10^{-6}$. The optical field distribution of the ADF is shown in Figure 7(b), where optical energy is coupled to the drop port for on-resonance wavelength of $\lambda_0 = 1534$ nm and then coupled primarily to the through port for off-resonance of $\lambda_0 = 1523$ nm. The time delay of about 200 ps is calculated from the normalized insertion phase with the on-resonance state (cf. Figure 7(b)), which is much larger than that achieved by homogenous

material based ADF resonator as depicted in Figure 5 for approximately the same size MRR. The time delay for flatness of $\pm 5\%$ error is about 407 GHz as depicted in Figure 7(c) that corresponds to the dispersive bandwidth of effective group index variation of about $\pm 2\%$ (cf. Figure 6(c)) around optical on-resonance wavelength of $\lambda_0 = 1534$ nm; as calculated using the homogenous modeling, the proposed ADF structure has an FSR of about 3.83 THz, where optical insertion loss variation of about 3.8 dB is experienced within the optical time delay range for various dispersive optical modes (cf. Figure 7(a)). Nevertheless, no performance degradation is predicted in SML technique because of a flat time delay, as shown in Figure 7(c).

3.2. Performance Estimation Using Hybrid Modeling

To meet the requirement of long optical delays in the ADF design, in the ADF design, the 2-D PhC with defect with a large radius ring waveguide should be selected. Nevertheless, the required simulation time is long (e.g., 1 hour for the structure shown in Figure 6(a) using Drexel ECE/COE server with meshing resolution of 20-nm) due to the complexity of the structure in an integrated circuit. Therefore, the proven hybrid modeling of time delay calculation for homogenous material based ADF resonators could be extended here to estimate the achievable time delay for the dispersive material based ADFs at a single wavelength (viz. by focusing only at on-resonance wavelength of 1534 nm). With the calculated effective group index in Figure 6(c), the designed radius of ring waveguide, simulated optical insertion loss as shown in Figure 7(a) and the time delay obtained by full-structure simulation shown in Figure 7(c), the coupling coefficient which is determined by the number of rows of dielectric rods between the defect bus waveguide and defect ring waveguide is predicted using Eq. (1) at the on-resonance wavelength as shown in Figure 8. Using the same analytical modeling of insertion phase from Eq. (1), the time delays of 2-D PhC ADF resonators with larger dimensions are then estimated, while other parameters remain unchanged. The estimated time delays of 6.6 ns, 13.2 ns, 26.3 ns, 45.6 ns, and 64.5 ns are for $R = 50$ μm, 100 μm, 200 μm, 350 μm, and 500 μm, respectively, as shown in Table 1.
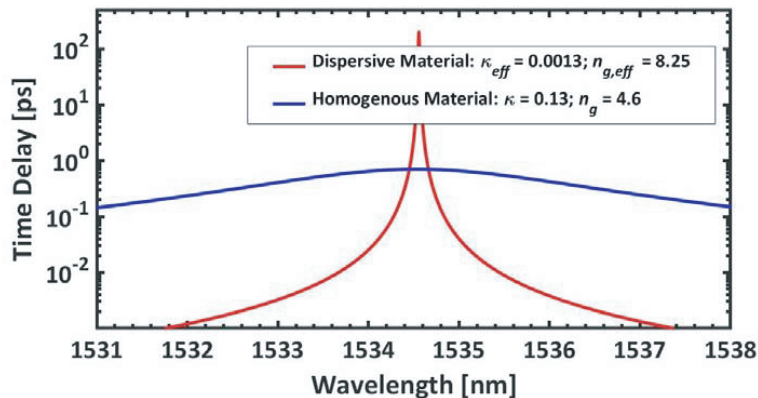
Figure 8. Estimated time delay of ADF resonator, (a) comparison of 2-D PhC based against the homogenous case for $R = 1.5$ μm at on-resonance wavelength of 1534 nm with inset showing magnified view for the homogenous case.

Note that the advantage of a larger radius MRR is not apparent when any irregularity in periodicity of 2-D PhC or rough surfaces of etched rods leads to additional optical waveguide loss of MRR, and it is beneficial to restrict radius to 100 μm in our case. Moreover, the calculated on-resonance wavelength slightly shifts with various radii of the defect based MRR waveguide; therefore, tuning range of on-resonance wavelength should also be considered for practical ADF design implementations with large R values [28].

Since the achieved time delay — as listed in Table 1 — is not linearly dependent on the radius R for the dispersive configuration, the cascaded 2-D PhC based ADF resonators (conceptually shown in Figure 9(a)) could be an option for attaining long optical time delays. Specifically a single ADF with

(a)

(b)
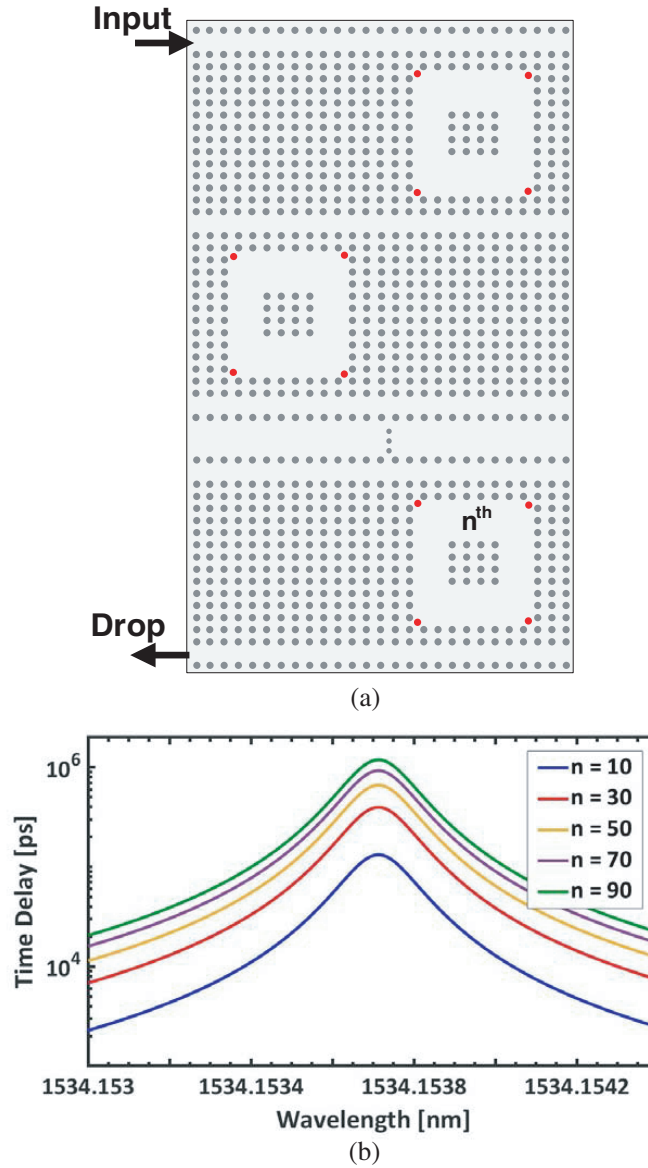
Figure 9. (a) Conceptual diagram of the n-cascaded 2-D PhC based ADF resonator structure with optical scatterers labeled in red dots at corners of MRR and (b) calculated time delay of cascaded ADF resonators of different order of n, where a total time delay as high as $1.2\,\mu$s and aggregate optical insertion loss of about $4\,$dB is attained at about $1534\,$nm for $n = 90$.

Table 1. Comparison of predicted optical delay and insertion loss for 2-D PhC ADF with various radii using the hybrid modeling at on-resonance of $1534\,$nm.

R [μm]	1.5	50	100	200	350	500
Time delay [ns]	0.2	6.6	13.2	26.3	45.6	64.5
Optical loss [dB]	0.040	0.042	0.045	0.070	0.113	0.231

$R = 100\,\mu$m is selected as the unit cell time delay of τ, and by cascading n of them a total time delay is calculated using Eq. (4) [7] while maintaining a smaller overall chip size with a reasonable optical loss of $0.045 \times n\,$dB. In the manufactured cascaded resonator structure, the individual parameters of each

MRR in the cascaded 2-D PhC based ADF might be slightly different from the one used in the hybrid modeling of a single resonator, but identical parameters are assumed for all the resonators for the sake of estimating the order of magnitude of the total time delays. The calculated optical time delay of about 925 ns is depicted in Figure 9(b) for $n = 70$ cascaded 2-D PhC based ADF resonators with the total optical loss of 3.15 dB.

$$H_{drop,\,cascaded} = \prod_{i=1}^{n} \frac{-\sqrt{(1-\gamma_{1i})\,\kappa_{1i}\,(1-\gamma_{2i})\,\kappa_{2i}}\;e^{-(\alpha_i L_i/4 + j\pi n_{g,i} L_i/\lambda)}}{1 - \sqrt{(1-\gamma_{1i})\,(1-\kappa_{1i})\,(1-\gamma_{2i})\,(1-\kappa_{2i})}\;e^{-(\alpha_i L_i/2 + j2\pi n_{g,i} L_i/\lambda)}} \tag{4}$$

Moreover, optical losses will influence the FSR transfer function [29]. For example, the achieved 3-dB optical bandwidth is about 1.6 GHz calculated by using the homogenous modeling for the case of $R = 1.5\,\mu$m, and high RF frequency modulated optical modes (e.g., X-band) cannot survive through the resonators. On the other hand, the actual dispersive wavelength response of a 2-D PhC based ADF resonator shown in Figure 6(c) and Figures 7(a) & (c) indicates that the modulated optical modes of 1533.921 and 1534.078 nm for chip level OEO [7, 30] with an intermodal oscillation of 10 GHz survive after passing through the drop port, but with slightly different optical attenuations of 0.08 dB and 0.05 dB, respectively. In practical designs, the guided optical mode partially leaks out of the line-defect to the wall of dielectric rods arrays with dielectric absorption that causes additional optical loss. Therefore, insertion loss differences between realistic lossy dielectric rods with complex index of refraction $n^c = n - jk$ (i.e., $k > 0$) and ideal loss-free cases (i.e., $k = 0$) are compared despite that the optical waveguiding in the 2-D PhC is entirely in air; even though SiO_2 and Si_3N_4 dielectric rods exhibit very small k values of complex index of refraction compared to Si, an upper bound for the excess loss is to be calculated for the worst case scenario of Si rods with $k = 0.001$. To estimate any additional excess optical losses, FDTD modeling of the ADF with $R = 1.5\,\mu$m is used as a baseline to compare. In the worst case of Si rods with $k = 0.001$, the optical field dropped through the ADF resonator is decreased with an excess optical loss of dielectric rods by about 0.3 dB. Therefore, the proposed cascaded resonator structure experiences an excess optical loss of about 21 dB; nonetheless, in practice semiconductor amplifiers (SOA) are suggested to compensate the optical loss experienced in longer optical delays before controlling free-running OEO [7].

4. CONCLUSIONS

On-chip optical time delay is a key component for achieving environmentally robust OEOs. The design and modeling of chip level ADF are presented here, and the achieved optical time delays are compared using a homogenous versus a 2-D PhC optical waveguide designs. Compared to other simulation methods of finite-element method (FEM), beam-propagation method (BPM) or method of moment (MOM), the most accurate modeling to explore the performance of the optical components is by means of full-wave 3D FDTD; nevertheless, the FDTD modeling method is excessively time-consuming when complex structures are considered. In particular, the required modeling time is well beyond most available computation resources when the dispersive ADF structures rely on the 2-D PhC resonators for long optical delays.

The focus of this paper is to develop a fast method using hybrid analytical and numerical modeling technique to estimate achieved optical time delays for MRRs with a long radius of 100 μm at the 1534 nm wavelength. The optical FDTD simulation was employed to predict the optimized design of MRR based on operating wavelength, optical insertion loss, and FSR to meet realization of the self-forced oscillation combined with the SML operation of a custom designed MML. Simulation method of bi-fold symmetry could help to reduce the required computational resources for FDTD simulation, while maintaining a high spatial resolution required for high accuracy numerical modeling of FDTD. Since the expected computational time for accurate modeling of the larger diameter MRR is significant using the available computational resources (e.g., CPU time of 60 min for a 2-D PhC ADF of 1.5 μm using a server with 11.1 GB RAM and Intel(R) Xeon(R) CPU E5-2699 v4 @ 2.2 GHz located at the ECE/COE of Drexel University), alternative modeling has been developed using a hybrid modeling approach presented here. Since the simulation time for full-wave modeling of a larger dimension ADF or the cascaded ADF structures is outside of the ECE/COE computation capability — particularly for the design using 2-D PhC with optical defect and lattice constant of $a = 500$ nm and filling factor $f = 0.177$, where the optical

scattering rods placed in key locations for reduced optical losses — the hybrid solution presented in this paper is introduced to facilitate design optimization in a reduced computation time. This proposed method relies on the key ADF parameters that are estimated from FDTD simulations to estimate both optical drop port time delay and amplitude calculation. Single ADF with $R = 100\,\mu m$ is considered as a suitable compromise of long optical time delay and low optical loss. 70 cascaded 2-D PhC ADF resonators with the radius of $100\,\mu m$ can achieve about $925\,ns$ delay, and the chip size is less than $0.4 \times 14\,mm^2$ using the proposed structure (cf. Figure 9(a)). Nonetheless, the fabrication of 2-D PhC defect waveguide could be somewhat labor intensive due to manufacturing challenges of maintaining periodicity over a large chip area.

The recent advances in neuromorphic software modeling [31, 32] could be utilized for such a challenging problem of numerical calculations of optimum chip level design of optical time delays based on larger diameter ADF based resonators. Alternatively analytical calculations could be performed with a specialized metamaterial design using inverse scattering problem [33]. In the absence of these forward-looking technologies a hybrid approach is the most realistic method of developing accurate predictions without significant numerical resources required for modeling of time delay in dispersive structures of 2-D PhC using ADF based resonators.

REFERENCES

1. Pérez, D., I. Gasulla, and J. Capmany, "Field-programmable photonic arrays," *Opt. Express*, Vol. 26, 27265–27278, 2018.

2. Smit, M., K. Williams, and J. van der Tol, "Past, present, and future of InP-based photonic integration," *APL Photon.*, Vol. 4, No. 5, Art. No. 050901, May 2019.

3. "JePPIX MPW Platforms", JePPIX, https://www.jeppix.eu/mpw-services/get-started/performance-summary-table/.

4. Liu, A. Y. and J. Bowers, "Photonic integration with epitaxial III–V on silicon," *IEEE Journal of Selected Topics in Quantum Electronics*, Vol. 24, No. 6, 1–12, Art No. 6000412, Nov.–Dec. 2018.

5. Daryoush, A. S., "Opto-electronically stabilized RF oscillators," *Microwave and Wireless Synthesizers: Theory and Design*, 701–759, 2nd Edition, Appendix F, John Wiley & Sons, Inc., 2021.

6. Yao, J., "Photonic integrated circuits for microwave photonics," *2017 IEEE Photonics Conference (IPC) Part II*, 1–2, Orlando, FL, 2017.

7. Wei, K. and A. S. Daryoush, "Self-injection locked oscillation of multi-mode laser in heterogeneously integrated silicon photonics," *The 2021 IEEE International Microwave Symposium (IMS)*, Atlanta, GA, June 6–11, 2021.

8. Hao, T., et al., "Recent advances in optoelectronic oscillators," *Advanced Photonics*, Vol. 2, No. 4, 044001, 2020.

9. Sun, T., K. Wei, and A. S. Daryoush, "Inter-modal laser based RF output stabilization using forced SILPLL technique," *2019 International Topical Meeting on Microwave Photonics (MWP)*, 1–3, Ottawa, ON, Canada, 2019.

10. Sun, T. and A. S. Daryoush, "Self-mode-locked multimode lasers for stabilized RF oscillators," *Electronics Lett.*, Vol. 55, No. 25, 1351–1353, December 2019.

11. Sun, T. and A. S. Daryoush, "RF frequency synthesizer based on self-mode-locked multimode lasers," *Journal of Lightwave Technology*, Vol. 38, No. 8, 2262–2270, April 15, 2020.

12. Daryoush, A. S., K. Wei, T. Sun, L. Zhang, U. L. Rohde, and A. K. Poddar, "Compact highly stable frequency synthesizers for integrated RF front-end," to appear in *Microwave Journal*, Vol. 64, No. 8, August 2021.

13. Sun, T., L. Zhang, K. Receveur, A. K. Poddar, U. L. Rohde, and A. Daryoush, "Integrated implementation of ultra-stable VCO using optical self-ILPLL techniques," *2016 IEEE MTT-S International Microwave Symposium (IMS)*, 1–4, 2016.

14. Daryoush, A. S. and T. Sun, "Multi-mode lasers for self-forced opto-electronic oscillators in compact frequency synthesizers," *IEEE Journal of Microwaves*, Vol. 1, No. 2, 625–638, Spring 2021.

15. Wei, K., "Photonic crystal enhanced electrooptic polymer based optical modulators for realization of integrated 40 Gs/s all-optical analog/digital converters with 8 effective number of bits," Ph.D. thesis, Drexel University, August 2021.

16. Shahoei, H., M. Li, and J. Yao, "Continuously tunable time delay using an optically pumped linear chirped fiber bragg grating," *Journal of Lightwave Technology*, Vol. 29, No. 10, 1465–1472, May 15, 2011.

17. Savchenkov, A. A., et al., "Whispering-gallery mode based opto-electronic oscillators," *2010 IEEE International Frequency Control Symposium*, 554–557, Newport Beach, CA, 2010.

18. Dai, J., et al., "Compact optoelectronic oscillator based on a Fabry-Perot resonant electro-optic modulator," *Chinese Optics Letters*, Vol. 14, No. 11, 110701, 2016.

19. Sun, T., "Forced oscillation in integrated opto-electronic circuits for realization of stable RF synthesizers," 2019.

20. Bogaerts, W., et al., "Silicon microring resonators," *Laser Photon. Rev.*, Vol. 6, No. 1, 47–73, 2012.

21. Bahadori, M., et al., "Design space exploration of microring resonators in silicon photonic interconnects: Impact of the ring curvature," *Journal of Lightwave Technology*, Vol. 36, No. 13, 2767–2782, July 1, 2018.

22. Zhang, L., A. K. Poddar, U. L. Rohde, and A. S. Daryoush, "Comparison of optical self-phase locked loop techniques for frequency stabilization of oscillators," *IEEE Photonics Journal*, Vol. 6, No. 5, 1–15, Art. No. 7903015, October 2014.

23. Bahadoran, M. and I. S. Amiri, "Double critical coupled ring resonator-based add-drop filter," *Journal of Theoretical and Applied Physics*, Vol. 13, 213–220, 2019.

24. Optiwave.s software OptiFDTD, Version 15.0.1: http:// https://optiwave.com/, Capella Court, Ottawa, 2020.

25. Girault, P., et al., "Integrated polymer micro-ring resonators for optical sensing applications," *J. Appl. Phys.*, Vol. 117, No. 10, Art. No. 104504, March 2015.

26. Talebi, N. and M. Shahabadi, "Analysis of a lossy microring using the generalized multipole technique," *Progress In Electromagnetics Research*, Vol. 66, 287–299, 2006.

27. Qiang, Z., W. Zhou, and R. A. Soref, "Optical add-drop filters based on photonic crystal ring resonators," *Opt. Expr.*, Vol. 15, 1823–1831, 2007.

28. Zhang, W. and J. Yao, "Photonic integrated field-programmable disk array signal processor," *Nat. Commun.*, Vol. 11, 406, 2020.

29. Takano, H., B. S. Song, T. Asano, and S. Noda, "Highly efficient multi-channel drop filter in a two-dimensional hetero photonic crystal," *Opt. Express*, Vol. 14, 3491–3496, April 2006.

30. Daryoush, A. S. and K. Wei, "Integrated opto-electronic chip as microwave and millmeter-wave frequency synthesizer," *US Provisional Patent Application: 63/209,247*, June 10, 2021.

31. Monroe, D., 2014, "Neuromorphic computing gets ready for the (really) big time," *Commun. ACM*, Vol. 57, No. 6, 13–15, June 2014.

32. Maan, A. K., D. A. Jayadevi, and A. P. James, "A survey of memristive threshold logic circuits," *IEEE Transactions on Neural Networks and Learning Systems*, Vol. 28, No. 8, 1734–1746, January 1, 2016.

33. Camacho, M., B. Edwards, and N. Engheta, "Simultaneous analog computing using multi-frequency inverse-designed metamaterial platforms," *2020 Conference on Lasers and Electro-Optics (CLEO)*, 1–2, 2020.